doi:10.22100/ijhs.v12i1.1302
Original Article

SJMS 2026;12(1):27-41
sjms.shmu.ac.ir

SJMS
Shahroud Journal of Medical Sciences

Comparative Evaluation of Graphene Oxide, Zinc Oxide, and Zinc Sulfide Nanoparticles in Carbomer-HPMC for Enhanced Wound Healing

Yousef Moradian Haftcheshmeh[1], Tahereh Sadat Tabatabai[1], Tayebeh Sadat Tabatabai[1], Majid Salehi[2,3], Amir Atashi[4], Vahid Shirshahi[4*]

[1] Student Research Committee, School of Medicine, Shahroud University of Medical Sciences, Shahroud, Iran.
[2] Regenerative Medicine Research Center, Shahroud University of Medical Sciences, Shahroud, Iran.
[3] Department of Tissue Engineering, School of Medicine, Shahroud University of Medical Sciences, Shahroud, Iran.
[4] Department of Basic Sciences, School of Medicine, Shahroud University of Medical Sciences, Shahroud, Iran.

Received: 13 July 2025
Accepted: 6 October 2025

Abstract

Background: *Wounds are treated using various approaches, including hydrogel dressings and nanoparticles (NPs). Hydrogel dressings provide a cooling effect that promotes wound healing, while NPs such as graphene oxide (GO), zinc oxide (ZnO), and zinc sulfide (ZnS) enhance cellular activity and accelerate the healing process. This study aimed to investigate the effects of GO, ZnS, and ZnO NPs loaded with carbomer 980 and HPMC polymers on wound healing.*

Methods: *The mechanical and physical properties of the scaffolds were evaluated using FTIR, SEM, pH monitoring, degradation rate, water absorption, blood clotting index (BCI), and hemolysis tests. Biocompatibility and cell migration were assessed via MTT assay, DAPI staining, and scratch tests. In addition, full-thickness (15 mm × 15 mm) wounds were created in animal models, and wound healing was evaluated using Verhoeff-Van Gieson and hematoxylin-eosin staining.*

Results: *GO-based hydrogels exhibited superior biocompatibility, wettability, controlled degradation, enhanced cell viability, and accelerated cell migration compared to ZnS- and ZnO-based formulations when combined with carbomer 980 and HPMC polymers. Histological analysis revealed increased collagen and elastin synthesis, enhanced angiogenesis, and greater epidermal thickness.*

Conclusions: *The prepared hydrogels show promising potential for wound healing applications. Further clinical studies are warranted to validate their therapeutic efficacy.*

Keywords: Carbomer, HPMC, GO NPs, ZnS NPs, ZnO NPs.
***Corresponding to:** V Shirshahi, **Email:** shirshahi@gmail.com

Please cite this paper as: Moradian Haftcheshmeh Y, Tabatabai TS, Tabatabai TS, Salehi Majid, Atashi A, Shirshahi V. Comparative Evaluation of Graphene Oxide, Zinc Oxide, and Zinc Sulfide Nanoparticles in Carbomer-HPMC for Enhanced Wound Healing. Shahroud Journal of Medical Sciences 2026;12(1):27-41.

Introduction

The wound healing process is carried out through various mechanisms such as blood coagulation, inflammation, angiogenesis, fibroplasia, epithelialization, contraction and regeneration. When wounds heal in an orderly manner and within a certain period of time, they are considered acute wounds. When wound healing is prolonged or occurs without achieving anatomical integrity, it is considered chronic wounds [1]. According to reports, managing exudate and maintaining moisture balance are two factors that should be taken into account when treating wounds [2, 3]. Proteases, matrix metalloproteases, and proinflammatory cytokines are all present in high concentrations in chronic wound exudate, and they all prevent chronic wound healing. As a result, maintaining the right balance of moisture in wounds is crucial. The use of absorbent medications, negative pressure therapy, different kinds of hydrogel and hydrocolloid dressings, nanotechnology and nanoparticles (NPs), etc. are common techniques for managing exudate and wound moisture [4]. In addition to absorbing wound exudate from the wound's surface, wound dressings need to keep the surrounding area moist. Hydrogels provide the moisture required for efficient wound healing because they swell when wet without disintegrating. Drug delivery and tissue engineering are the primary applications for hydrogels, which are networks of polymer molecules with water holes. Combining materials like NPs or nanogels with hydrogels to enhance their characteristics is known as nano-hybrid hydrogels. These mixtures increase the hydrogels' drug-loading capacity and make them particularly appropriate for lipophilic medications. There is evidence that NPs can improve herbal medications' stability, bioavailability, and solubility [5].

Among the polymers that can be used to prepare hydrogels are carbomer 980 and hydroxypropyl methylcellulose (HPMC).

The high molecular weight polymer carbomer 980 is made up of acrylic acid units that have been cross-linked using polyacrylic alkyl ethers. They are heavily interlaced molecules in the solid state that start to unfold when submerged in water. With a pH of roughly 2.5 and a dissociation constant of pKa=6, carbomer particles floating in water are regarded as weak acids. According to reports, carbomer has been utilized extensively in wound healing due to its great gelling capacity [6].

Adding hydroxypropyl and methoxy groups to cellulose chains yields HPMC, a cellulose-derived polymer that finds extensive application in a variety of sectors, including the food, cosmetic, pharmaceutical, and health industries. This polymer's molecular weight and the amount of methoxy and hydroxypropyl groups it contains have a significant impact on its physicochemical characteristics [7]. One of the most significant characteristics of this polymer is its great swelling ability, which has resulted in its extensive application in drug administration since the polymer chains relax when it comes into contact with biological fluids or water, releasing the drug [8].

Based on the advances made, NPs have wide applicability for wound healing. One of the reasons for this is directly

related to the size of the NPs because NPs have a higher surface-to-volume ratio, which leads to different mechanical, chemical, electrical, optical and magnetic properties compared to the bulk material [9]. Numerous NP kinds are in widespread usage, such as graphene oxide (GO), zinc oxide (ZnO) and zinc sulfide (ZnS).

ZnO NPs, which are used in a wide range of applications such as energy storage, nanosensors, cosmetics, etc., have unique properties such as semiconducting, piezoelectric, and optical properties. These particles are also regarded as low-toxicity, biocompatible materials [10]. In animal investigations, these NPs have demonstrated a high capacity for epithelial regeneration [11] and a beneficial function in wound healing [12].

With a broad optical band gap, ZnS NPs, a group II–IV semiconductor, are a desirable substance. These NPs are produced using a variety of techniques, including sol-gel, sputtering, microwave irradiation, and ultrasonic irradiation. They are known to have two crystal structures: cubic and wurtzite. They can be utilized as one of the commonly used phosphors for cathode ray tubes, field emission displays, and luminescent material.

In 2004, mechanical exfoliation was used to create graphene. The structure of this substance, which is a single layer with a thickness of one atom, is formed exclusively of carbon atoms, and all atoms are in sp^2 hybridization [13, 14]. Each carbon atom in this configuration forms a unique honeycomb structure by bonding with three other carbon atoms [15]. Studies show that adding these NPs to hydrogel dressings results in homogeneous, porous, and linked structures that improve the dressings' mechanical qualities and have good water absorption capabilities [16, 17].

Considering the aforementioned materials, the aim of this study is to compare the effects of GO, ZnO, and ZnS NPs loaded with carbomer 980 and HPMC polymers on the wound healing process in vitro and in vivo.

Materials and Methods

Materials: This study utilized primary materials obtained from reputable suppliers to ensure the consistency and reliability of experimental results. Hydrochloric acid (HCl), and sulfuric acid (H_2SO_4) were sourced from Merck, Germany. Graphite powder along with ammonia, hydrogen peroxide (H_2O_2), and potassium permanganate ($KMnO_4$), were purchased from Acros Organics, Belgium. For biological assessments, mouse fibroblast cells (3T3) were obtained from the Pasteur Institute of Iran. Carbomer 980 (Pharmaceutical grade) was purchased from Sigma-Aldrich (Merck, Germany), HPMC (Pharmaceutical grade, Sigma-Aldrich, USA) was used as received, and ZnO/ZnS NPs were obtained from US Research Nanomaterials, Inc.

Synthesis of GO NPs: A modified Hummer's technique was used to synthesize GO [18]. GO was synthesized using a modified Hummer's method. Graphite powder was mixed with H_2SO_4 and stirred for 3 hours. $KMnO_4$ was added in an ice bath, followed by gradual heating and stirring at 40°C, 70°C, and finally 105°C, with intermittent additions of distilled water. Afterward, H_2O_2 and more water were added. The resulting mixture was centrifuged, and the solid was washed with 5% HCl and distilled water until neutral [14].

Hydrogel preparation: First, distilled water was used to dissolve carbomer 980 (1% w/v) and HPMC (0.5% w/v) to create solutions. After that, the two solutions were mixed together. Next, the solution containing carbomer 980 and HPMC was supplemented with GO NPs (0.05%w/v), ZnO (5%w/v), and ZnS (1%w/v). To create the hydrogel, the resultant solution was agitated with a homogenizer for ten minutes and exposed to ultrasound for ten minutes.

Morphology and structure observation: Scanning electron microscopy (SEM) was used to examine the samples' morphology and structure (Hitachi, Japan). After a sputter coating was applied, the samples were mounted on sample holders and put inside a SEM chamber. Digital pictures were taken. Image J software was used to evaluate the pore size and determine the average pore size.

FTIR spectra measurements: To evaluate the functional groups of the samples and the interactions in the produced scaffold, Fourier transform infrared spectroscopy (FTIR) was performed using a Bruker Equinox 55LS 101 series instrument (Germany) with an adjustable resolution of 4 cm^{-1} throughout the 400–4000 cm^{-1} range.

Cell viability: The basis of this test is the capacity of living cells to use mitochondrial enzymes to convert yellow tetrazolium salt (MTT) into insoluble purple formazan crystals. 3T3 cells were cultivated in order to examine the cytotoxicity and material biocompatibility of the samples. In 96-well plates, 7×10^3 cells were planted onto each scaffold. Cell viability and proliferation were assessed using the 3-(4, 5-dimethylthiazol-2-yl)-2, 5-diphenyltetrazolium bromide (MTT) test at 48 and 72 hours of incubation. Fresh medium containing 10% MTT solution (5 mg/mL) was added to the culture medium at the designated intervals. After that, the cells were shielded from light and incubated for two hours at 37 ^{0}C. Dimethyl sulfoxide (DMSO) was added to the medium after the incubation period in order to dissolve the purple formazan crystals that had developed. A microplate reader from Awareness Technology was used to measure the samples' optical absorbance at 570 nm. Lastly, the following formula was used to determine the cell viability rate.

$$\text{Cell viability (\%)} = \frac{\text{OD Sample}}{\text{OD Positive Control}} \times 100$$

Anti-inflammatory test: The degree of tissue damage and protein structural alterations can be evaluated in vitro with the anti-inflammatory test. 2.8 milliliters of PBS (pH=6.8) and 0.2 milliliters of 1% albumin are combined with 0.1 grams of the sample for this purpose. After 15 minutes of incubation at 37°C, the mixture is heated for five minutes at 70°C. At 660 nm, absorbance is finally measured. This procedure uses aspirin as the standard and PBS + 1% albumin as the control.

$$\text{Protein denaturation} = \frac{A_{\text{Control}} - A_{\text{Sample}}}{A_{\text{Control}}} \times 100$$

Total antioxidant capacity test: The ability of tissues to fight off free radicals and reactive oxygen species (ROS) is gauged by the total antioxidant capacity index of biological samples or skin. In research pertaining to skin care, cosmetics, and skin disorders, a higher antioxidant capacity indicates the skin's increased power to shield cells from oxidative stress. In this context, the antioxidant reagent ABTS is mixed with cell extract that has been extracted from skin tissue. Next, a spectrophotometer set to 734 nm is used to measure the solution's color change. This measurement aids in determining the sample's antioxidant capability.

Lactate Dehydrogenase Assay: Since lactate dehydrogenase (LDH) leaks out of injured cells, this test is frequently used to evaluate cell damage or damage to the cell membrane. Cell death or injury is indicated by elevated LDH levels in the extracellular fluid. In this investigation, the LDH activity assay was used to measure the rate of cell death on the hydrogels 72 hours after the original cell seeding. After 15 minutes, the color change was measured at 450 nm using a microplate spectrophotometer.

Blood compatibility test: BC testing known as blood compatibility testing, looks at a substance's ability to cause negative blood reactions such hemolysis. 2.5 mL of regular saline was used to dilute 2 mL of fresh anticoagulated human blood for this test. The samples were then mixed with 0.2 mL of the diluted blood. After 60 minutes at 37 ^{0}C, the mixture was centrifuged for 10 minutes at 1500 rpm. After the produced supernatant was moved to a 96-well plate, the Anthos 2020 (Biochrom, Berlin, Germany) microplate reader was used to measure the absorbance at 545 nm. 0.2 mL of diluted blood in 10 mL of deionized water served as the positive control, while 0.2 mL of diluted blood in 10 mL of normal saline served as the negative control. Ultimately, the following formula was used to determine the degree of hemolysis:

$$\text{Hemolysis \%} = \frac{\text{Dt - Dnc}}{\text{Dpc - Dnc}} \times 100$$

Where Dt shows the optical density of the sample, Dnc indicates the optical density of the negative control, and Dpc is the absorbance of the positive control.

Blood clotting index: The purpose of this test is to determine whether coming into touch with different materials will cause blood to clot. After being sliced into disk shapes, the samples were put in beakers. The beakers were then submerged for an hour at 37°C in a water bath. Each sample was then supplemented with 100 µL of blood containing the anticoagulant. Five minutes later, 20 µL of a calcium chloride solution containing 0.2 mol/l was added. Five minutes later, the samples were carefully mixed with 25 milliliters of distilled water. For five minutes, the samples were maintained at 37°C. At 545 nm, their absorbance was lastly measured. 100 µL of blood and 25 ml of distilled water (no sample) were included in the control group. The following formula was used to determine the blood clotting index (BCI):

$$\text{BCI} = \frac{\text{A sample}}{\text{A control}} \times 100$$

Where A sample is the absorbance value of each sample and A control is the absorbance value of the control group.

Blood uptake test: Blood Uptake testing is frequently used in tissue engineering and biological research to evaluate how chemicals interact with blood. This test measures the rate of absorption or the amount of physical change in the blood sample after a material meant to come into contact with the blood is left in contact with the blood for a predetermined amount of time. At room temperature, the samples were submerged in whole human blood every ten and twenty minutes. Following measurements of the beginning weight (W0) and moist weight (W1), the blood uptake capacity was computed as follows:

$$\text{Blood uptake capacity} = \frac{\text{W1 - W0}}{\text{W1}} \times 100$$

PH assessment: This test measures a solution's acidity or alkalinity, which can reveal how quickly its pH changes over time. The PH test was run for 2, 4, 6, 12, and 36 hours. Samples of the same weight were submerged in PBS for this experiment. A pH meter (pH meter 1140; Mettler Toledo, Greisensee, Switzerland) was used to test PH fluctuations once a week.

DAPI test: The structure of the cell nucleus can be examined using the staining technique known as the DAPI (4',6-diamidino-2-phenylindole) test. When exposed to UV light, the fluorescent dye DAPI attaches to DNA and releases blue light. In this research Cells were fixed 24 hours after seeding by submerging the samples for 8 minutes in a 4% paraformaldehyde solution. After 10 minutes in a Triton X-100 (0.1%) solution to improve dye penetration to cells, samples were rinsed three times with PBS. Next, 50 µL of room-temperature DAPI staining solution was added to each well. The scaffolds were cleaned three times with PBS after the color was removed after five minutes. To maintain cell hydration, 50 microliters of PBS were supplied to each well. A fluorescent microscope was used to view the cells at an excitation wavelength of 358 nm and an emission wavelength of 461 nm.

Weight loss test: A scientific technique for assessing a material's stability or rate of degradation under particular environmental circumstances is the weight loss test. After precisely measuring the sample's starting weight (W0), it is put in a physiological environment or other body-like setting for a predetermined amount of time. After being submerged in 10 milliliters of regular saline, the samples were put in a closed oven at 37°C. to replicate circumstances that are comparable to those found in the body. Following the measurement of the samples' secondary weight (Wt), the samples' rate of degradation was determined using the formula below after two and four hours.

$$\text{Weight loss} = \frac{\text{W0 - Wt}}{\text{W1}} \times 100$$

Water absorption test: After being weighed, the lyophilized samples were submerged entirely in a beaker filled with phosphate buffered saline (PBS) at a pH of 7.4. At 30°C, immersion was carried out at predetermined intervals of two

and four hours. Following a speedy extraction and weighing of the samples, the water absorption rate of the samples was computed using the formula below:

$$\text{Equilibrium mass swelling (\%)} = \frac{M1\text{-}M0}{M0} \times 100$$

M_0 indicates the mass of the hydrogel in its dried state, while M_1 represents the mass of the hydrogel when it is expanded.

Cell migration test: A laboratory technique called the Wound Scratch Test is used to evaluate a cell's capacity to migrate and repair cellular wounds. To evaluate the migration of 3T3 cells, a wound-healing test was performed by scratching the confluent culture. On a six-well plate, cells were planted at a density of 5×10^3 3T3. The culture was maintained until roughly 80% confluence, and the medium was switched every two days. After removing the medium, a micropipette tip was used to create a scratch. The prescribed dosages of ESM were then administered to the cultures. Cells without any supplements were used as a control. The migration photos were captured using an Inverted Leica Fluorescence Microscope after being cultured for 12, 24, and 48 hours. The distance of the healed scratch was measured to determine the migration's magnitude (formula below).

$$\text{Healing (\%)} = \frac{\text{Area of Original Wound-Area of Wound during Healing}}{\text{Area of Original Wound}} \times 100$$

Surgical protocol: Animal research carried out in compliance with ethical norms have been authorized by Shahroud Medical University's ethics committee (IR.SHMU.REC.1401.166). Six healthy adult male Wistar rats weighing between 200 and 220 g each were given an intraperitoneal injection of xylazine (10 mg/kg) and ketamine (100 mg/kg) to induce anesthesia. As a consequence, the precise site of the wound was selected, and its measurements of 15 x 15 mm2 were removed, completely removing the wound's thickness. Six Wistar rats were split up into six groups for this investigation. Different drugs, including a negative control, were administered to each group. Positive control, treatment group (sample with GO, ZnO, ZnS NPs, and carbomer HPMC polymer). An elastic adhesive bandage and aseptic gauze were then used to implant the samples on the site of injury.37 At 14 days following the surgery, the pace of wound healing was assessed using a digital camera made by Tokyo, Japan-based Canon Inc., which recorded the wound's shrinkage. The % decrease in wound area at days 7, 10, and 14 was used to gauge the degree of wound closure. A stationary camera that tracked the wound margin on a 10-cm scale took pictures of the wound area. Image J software was then used to measure the wound reduction area. The following formula was then used to determine the percentage of wound closure.

$$Cn = \frac{A0 - An}{A0} \times 100$$

Hematoxylin-eosin and Verhoeff-Van Gieson: One method that is frequently used in histology to examine and analyze different bodily tissues is hematoxylin-eosin (H&E) staining. The Verhoeff-Van Gieson (VVG) staining technique is another crucial way to identify collagen and elastic fibers. According to this method, collagen is stained red by Van Gieson's dye, while elastic fibers are stained black by Verhoeff's dye, leaving other tissues looking yellow or brown. The animals were put to death using xylazine (20 mg/kg body weight) and ketamine (200 mg/kg body weight) fourteen days following treatment. Tissues from the skin were gathered and preserved in 10% formalin (pH 7.26). The tissues were divided into 5 µm slices and stained with both H&E and VVG techniques after 48 hours. An impartial reviewer used a light microscope (BX51; Olympus, Tokyo, Japan) with a digital camera (DP72; Olympus) to measure the production of granulation tissue, angiogenesis, fibroplasia, and epithelialization in various groups. The reviewer took pictures at 40x, 100x, and 400x magnification.

Animal ethics statement: All animal experiments and biological assessments in this study were conducted in strict accordance with the guidelines of the ARRIVE (Animal Research: Reporting of In Vivo Experiments), the U.K. Animals (Scientific Procedures) Act, 1986, EU Directive 2010/63/EU for animal experiments, and the National Institutes of Health Guide for the Care and Use of Laboratory Animals (NIH Publications No. 8023, revised 1978). The experimental protocol was approved by the Shahroud University of Medical Sciences (Approval Number: IR.SHMU.REC.1401.166).

Statistical analyses: Data analysis was performed using SPSS statistical software (version 26.0). Graphs were constructed using GraphPad Prism 8.0 (GraphPad Software, San Diego, CA, USA). Statistical significance was determined by a one-way ANOVA followed by the LSD post hoc test. P-value<0.05 were acknowledged as statistically significant.

Results

SEM results: Figure 1 (I) shows SEM images of the studied groups. All hydrogels have porous structures with interconnected pores. Measurements performed showed that the pore sizes of carbomer 980 (Figure 1A) and HPMC (Figure 1B) hydrogels were 23.93±18.10 and 10.25±5.75 µm, respectively. This size distribution indicates the presence of diverse porosities in the carbomer 980 structure and pores with smaller sizes and relatively more uniform distribution in the HPMC structure. As can be seen in Figure 1C, adding GO NPs to the carbomer 980 and HPMC mixture resulted in a uniform distribution of these particles in the polymer matrix and also increased the specific surface area in this mixture. Figures 1D and 1E also show the distribution of ZnO and ZnS NPs in the polymer matrix. In Figure 1F, the simultaneous incorporation of GO, ZnO, and ZnS NPs resulted in a structure with irregular porosity and reduced network integrity of the hydrogel. These results indicate that the simultaneous addition of ZnO and ZnS to GO-containing hydrogels can have negative effects on the hydrogel structure, which is likely due to the incompatible interaction between the NPs and the polymer matrix.

FTIR test results: Figure 1 (II) shows the FT-IR spectra of the studied groups. The red spectrum shows the characteristic peaks of the carbomer hydrogel. The peak observed at 809.92 cm^{-1} indicates the out-of-plane C-H vibrations of the methylene (CH_2) groups in the polyacrylate segments of the carbomer polymer. At a wavelength of 1230.23 cm^{-1}, C-H bending

vibrations of methyl groups (CH_3), at 1693.53 cm^{-1}, C=O stretching vibrations (carbonyl), at 2933.0307 cm^{-1}, C-H stretching vibrations of methylene and methyl groups are observed. The green spectrum shows the characteristic peaks of HPMC hydrogel. The peak at 940.23cm^{-1} represents the C-O-C stretching vibrations in ether groups or the C-H bending vibrations in methylene and methyl groups. This peak can also represent the vibrations of glycosidic rings in the polysaccharide structure of HPMC. The peak at 1218.6cm^{-1} represents the C-O stretching vibrations in ester or ether groups. It can also represent the C-H bending vibrations in methylene or methyl groups. C-H bending vibrations are seen, at 1668.769cm^{-1}, C=O stretching vibrations, at 2900.769cm^{-1}, C-H stretching vibrations, and at 3404.23cm^{-1}, hydroxyl group stretching vibrations are seen. The purple spectrum shows the characteristic peaks of carbomer and HPMC hydrogels containing GO NPs. The peak at 1135.69 cm^{-1} represents the O-H stretching vibrations in hydroxyl groups, the peak at 1479.23 cm^{-1} represents the C-H bending vibrations in methylene and methyl groups, the peak at 1633.230 cm^{-1} represents the C=C stretching vibrations or amide groups, indicating the presence of a double bond in the structure of the compound. The peak at 2918.53 cm^{-1} represents the C-H stretching vibrations in methyl and methylene groups, and the peak at 3404.230 cm^{-1} represents the O-H stretching vibrations, indicating the presence of hydroxyl groups in the structure and also the presence of moisture or hydrogen bonding. The characteristic peaks of carbomer 980, HPMC and ZnO NPs hydrogels are displayed in the yellow spectrum. Peak 863.230 cm^{-1} indicates the bending vibrations of C-H groups, peak 1058.692 cm^{-1}, the stretching vibrations of C-O bond, peak 1402.23 cm^{-1}, the bending vibrations of CH_2 groups, peak 2930.384 cm^{-1}, the stretching vibrations of C-H bond and peak 3392.384 cm^{-1}, the stretching vibrations of O-H bond and the presence of hydroxyl groups. The blue spectrum of the characteristic peaks of carbomer 980 and HPMC hydrogels containing ZnS NPs is shown. The peak at 815.84 cm^{-1} represents the bending vibrations of the S-H groups in ZnS NPs, the peak at 1052.769 cm^{-1} represents the stretching vibrations of the C-O bond, the peak at 1668.769 cm^{-1} represents the stretching vibrations of the C=O bond, the peak at 2924.461 cm^{-1} represents the stretching vibrations of the C-H bond and the peak at 3392.384 cm^{-1} represents the stretching vibrations of the O-H bond. In the black spectrum, which shows the characteristic peaks of carbomer 980 and HPMC hydrogels containing GO, ZnO and ZnS NPs, the peaks at 1052.769 cm^{-1} are the stretching vibrations of the C-O bond, the peak at 1491.076 cm^{-1} is the bending vibrations of the CH_2 bonds, the peak at 2924.461 cm^{-1} is the stretching vibrations of the C-H bond and the peak at 3404.230 cm^{-1} is the stretching vibrations of the O-H bonds.

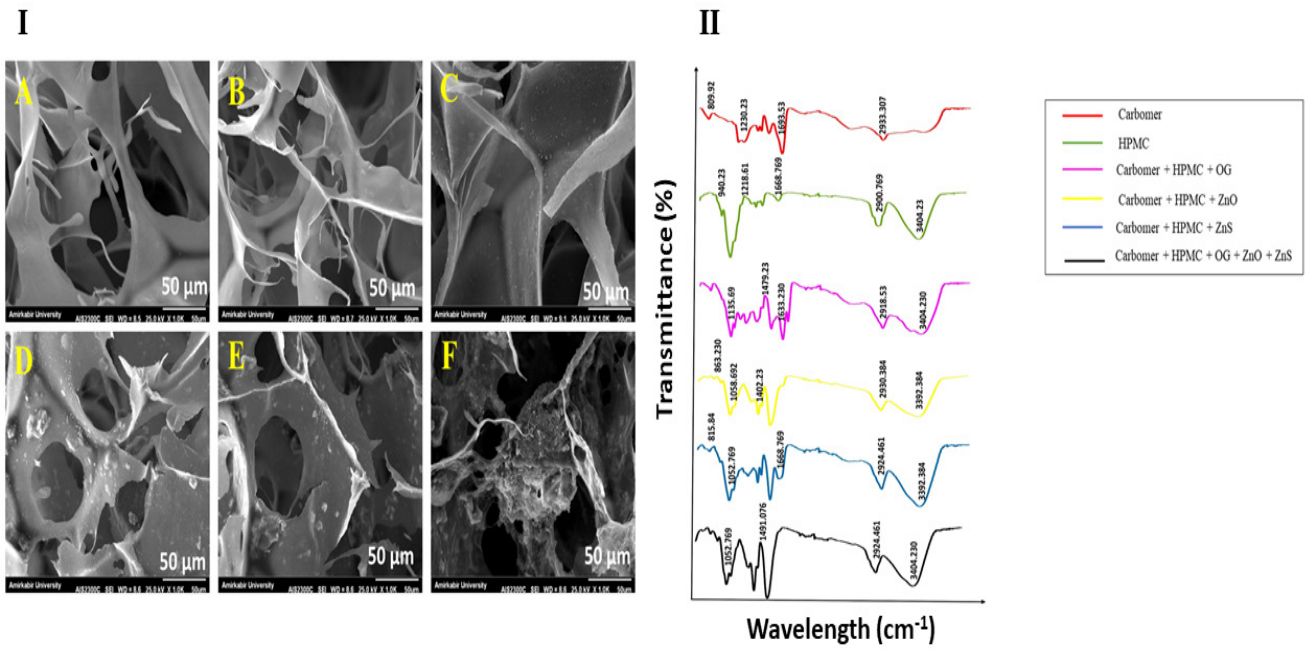

Figure 1 (I). Electron microscope images A: Carbomer 980. B: HPMC. Carbomer 980 and HPMC containing C: GO NPs. D: ZnO NPs. E: ZnS NPs and F: Combination of Carbomer 980, HPMC, GO, ZnO, ZnS (II): FT-IR spectra of the studied groups.

MTT test: Based on the analysis of the results obtained from the MTT test (Figure 2A), the proliferation and survival of 3T3 cells were evaluated after 24 and 72 hours of cell culture. The results indicate that after 24 and 72 hours, the survival rate of cells after treatment with a combination of carbomer 980, HPMC, GO NPs, ZnO and ZnS has significantly increased compared to other groups.

Anti-inflammatory test: The results of the anti-inflammatory test (Figure 2B), indicate that the carbomer 980 polymer has a higher anti-inflammatory effect than the HPMC

polymer, and both polymers show a significant decrease compared to the sixth group. Also, there is no significant difference between the anti-inflammatory effect of the three NPs of GO, ZnO and Zns compared to each other. However, when carbomer 980, HPMC, GO, ZnO and ZnS are combined together, due to the synergistic effect they have with each other, the anti-inflammatory effect is significantly increased and has a significant increase compared to the other groups.

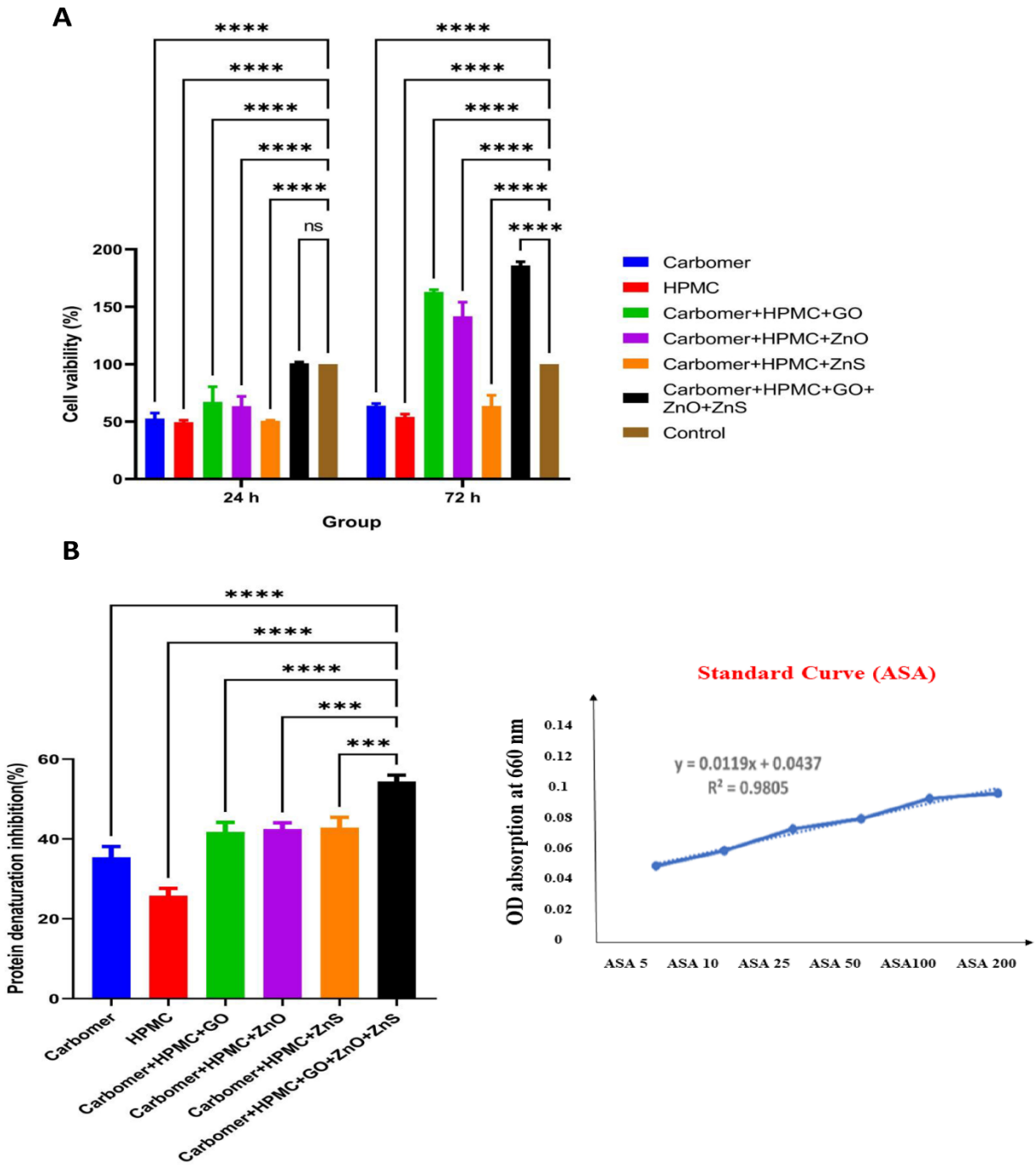

Figure 2. A: The effect of different groups on cell viability. B: Examination of the inhibition of protein degradation in the studied groups (**P-value<0.0001)**

LDH test: Based on the results obtained from the LDH test, (Figure 3A), the level of LDH released from cells treated with carbomer 980 and HPMC polymers is not significantly different from each other and does not increase significantly compared to the control group. However, the combination of these two polymers with GO NPs caused a decrease in the level of LDH released from cells and there was a significant decrease compared to the control group. However, when carbomer 980 and HPMC were combined with ZnO and ZnS NPs, the level of LDH increased significantly compared to the other groups. Also, according to the graph, it was found that the combination of three GO NPs, ZnO and ZnS with carbomer 980 and HPMC polymers significantly reduced the level of LDH released compared to the other groups and the control group.

TAC test: In this study, the results of the total antioxidant capacity test (Figure 3B) indicate that the two polymers carbomer 980 and HPMC and their combination with ZnO and ZnS NPs have almost similar antioxidant capacity, but when carbomer 980 and HPMC are combined with GO NPs, this capacity increases. Also, the combination of the sixth group, namely carbomer 980, HPMC, GO, ZnO and ZnS, due to the synergistic effect of these compounds, has significantly increased this capacity compared to other groups.

Blood compatibility: In Figure 3C, the results of the blood compatibility test indicate that between the two polymers carbomer 980 and HPMC, carbomer 980 has a higher blood compatibility. Also, no significant difference is seen between groups 3, 4, and 5. However, when combining the two polymers carbomer 980 and HPMC, as well as GO NPs, ZnO, and ZnS, the highest blood compatibility is observed compared to the control group. The reason for this is due to the synergistic effects of the compounds.

BCI Index: Based on the blood compatibility index test (Figure 3D), carbomer 980 has higher blood compatibility than HPMC (significant decrease compared to HPMC). Also, the combination of carbomer 980 and HPMC with GO NPs resulted in higher blood compatibility compared to the fourth and fifth groups (significant decrease). The combination of all NPs, namely GO NPs, ZnO and ZnS with the two polymers carbomer 980 and HPMC resulted in the highest level of blood compatibility observed in this group (significant decrease compared to the control group and other groups).

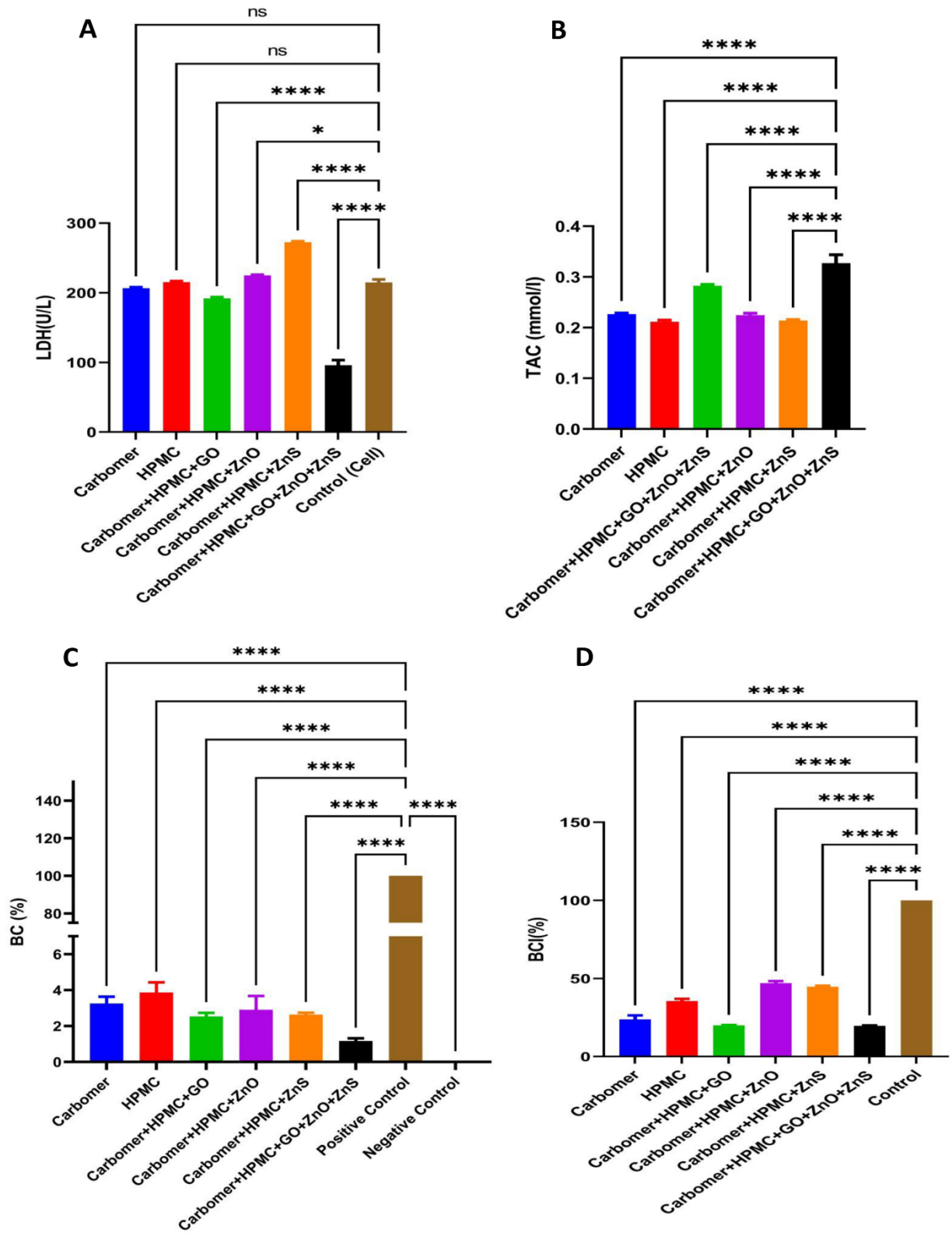

Figure 3. A: Comparison of the level of released LDH. B: Total antioxidant capacity in the study groups. C: Hemolysis rate of red blood cells. D: Blood compatibility rate of the study groups

(**P-value<0.0001)**

Blood uptake test: As can be seen in Figure 4A, carbomer 980 and HPMC alone have moderate blood absorption capacity and do not increase or decrease significantly compared to each other, but this capacity increases when combined with GO, ZnO and ZnS NPs. This is due to the nanostructure and high specific surface area in the groups containing NPs. In addition, in the latter group, the blood absorption capacity has increased significantly. This significant increase can be attributed to the synergistic effect between GO, ZnO and ZnS NPs. GO increases the ability to absorb liquids due to its nanostructure and high specific surface area. On the other hand, ZnO and ZnS can also help improve the absorption capacity due to their absorption and porosity properties. The combination of these NPs has probably led to the creation of a structure with greater porosity and a denser network that allows the absorption of a larger volume of blood.

pH test: The pH of the different samples at 2, 4, 6, 12 and 36 hours (Figure 4B) showed that there was no significant difference in pH values between the groups. These results indicate that the addition of compounds such as GO, ZnO and ZnS to the base formulation (carbomer 980 and HPMC) did not have a significant effect on the final pH of the product. Therefore, it can be concluded that these compounds are pH stable and do not cause significant changes in acidity or alkalinity.

Measuring the rate of degradation: Figure 4C shows the percentage of weight loss of the studied groups. Analysis of the results shows that in the time intervals of 2 and 4 hours, the rate of degradation and weight loss of the sixth group, i.e. the combination of carbomer 980, HPMC, GO, ZnO and ZnS, was the highest compared to the other groups and showed a significant increase.

Measuring water absorption: Based on the results presented in Figure 4D, in this study, the amount of water absorption in the time intervals of 2 and 4 hours indicates that the combination of carbomer 980 and HPMC with GO NPs, ZnO, and ZnS increased the water absorption capacity in this group compared to other groups, indicating a significant increase in water absorption compared to other groups.

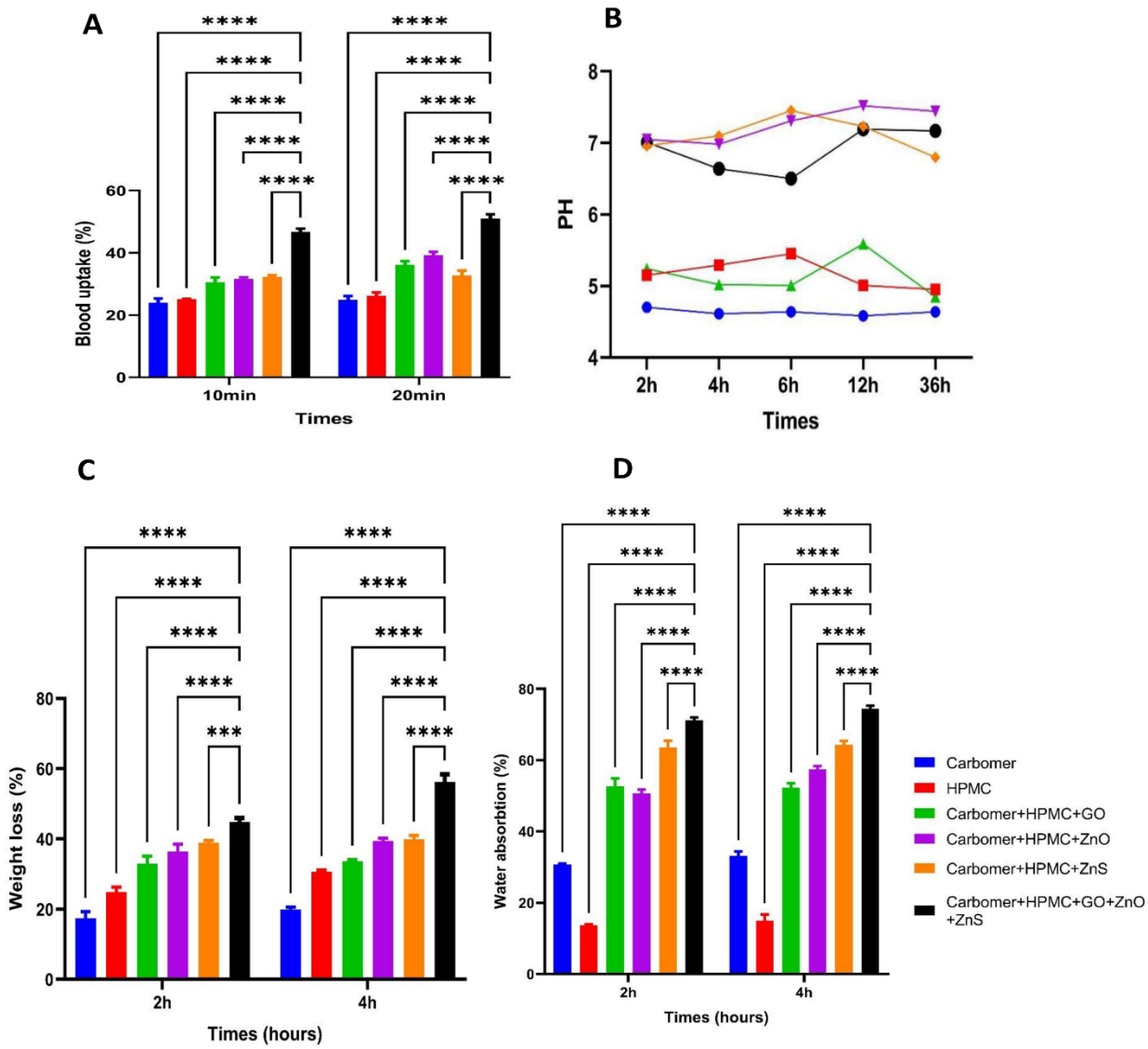

Figure 4. A: Comparison of blood absorption capacity in different groups. B: Comparison of pH values between different groups. C: Water absorption and D: Degradation rate of the studied groups

(**P-value<0.0001)**

Results of the DAPI test: To investigate and evaluate the health of the cell nucleus, DAPI staining (Figure 5) was used in this study. Analysis of the results showed that carbomer 980 and HPMC polymers alone performed well maintaining cell health. Also, by combining these polymers with GO, ZnO, and ZnS NPs, this capacity increased significantly. In addition, when carbomer 980 and HPMC were combined with all NPs, they performed exceptionally well in maintaining cell health, and the best results were observed in this group with the highest number of healthy cell nuclei.

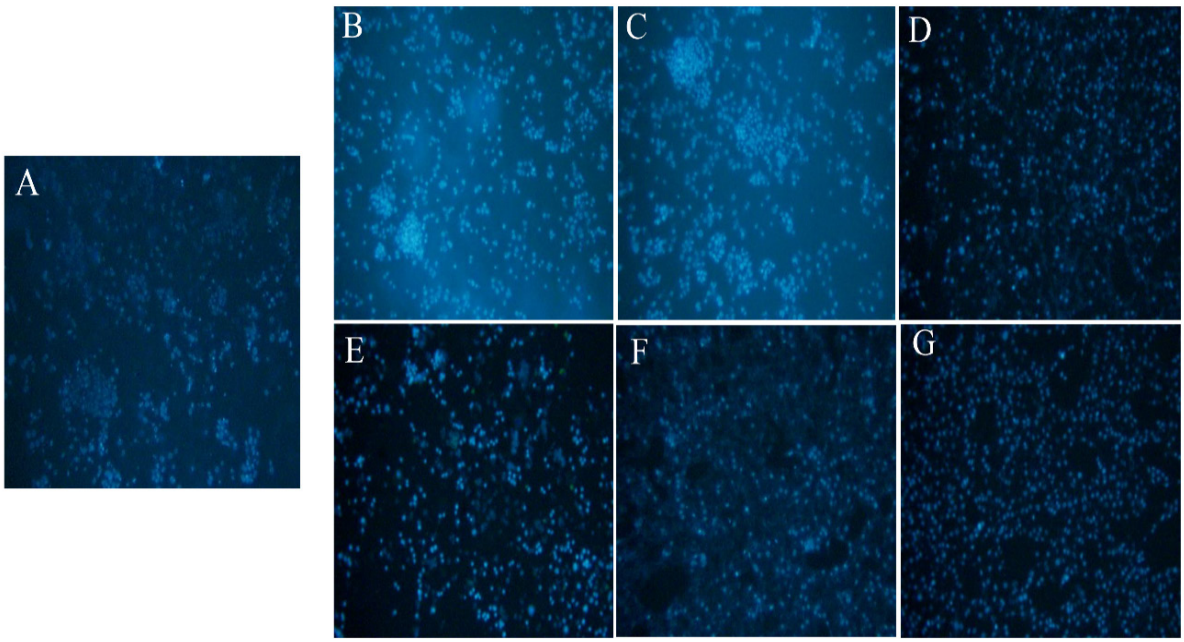

Figure 5. DAPI test results of the study groups. A: Control group. B: Carbomer 980. C: HPMC. D: Combination of carbomer 980 and HPMC with GO NPs. E: Combination of carbomer 980 and HPMC with ZnO NPs. F: Combination of carbomer 980 and HPMC with ZnS NPs. G: Combination of carbomer 980 and HPMC with GO, ZnO and ZnS NPs (40X).

Results of the in vitro cell migration: Based on the results obtained from the cell migration test, which is indicated in Figure 6, in cells treated with carbomer 980 and HPMC containing GO NPs, ZnO and ZnS, the scratched area formed in this group was significantly reduced compared to other groups at time intervals of 24, 48 and 72 hours.

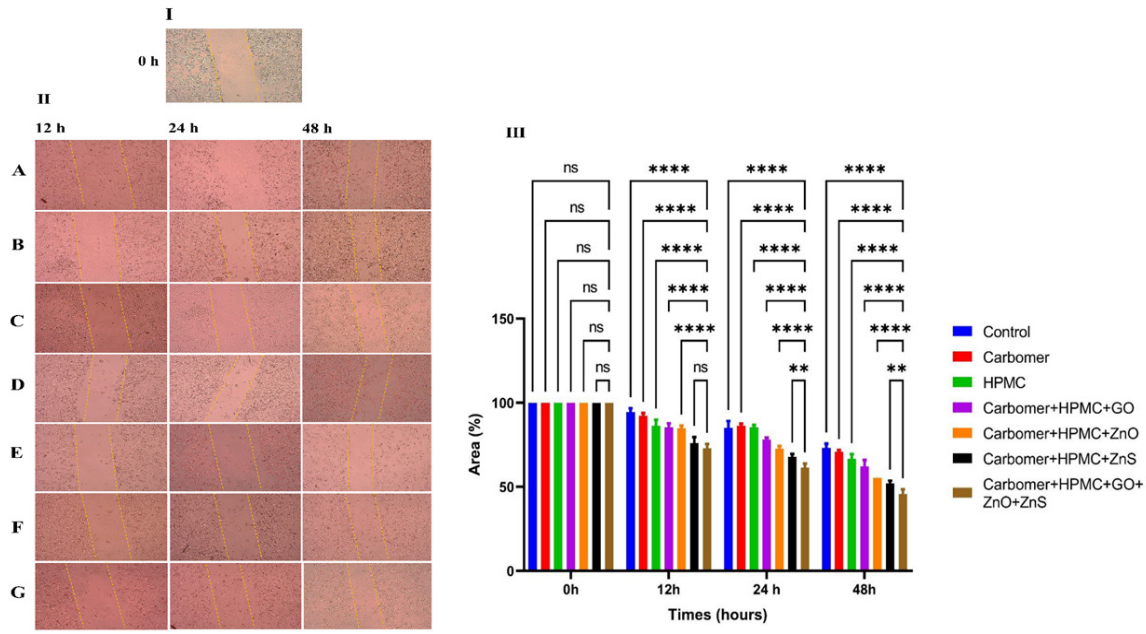

Figure 6. Cell migration study. I: Control group. II: Cell migration results of the studied groups at 12, 24 and 48 hours. III: Cell migration experiment diagram of the studied groups (40X)

(**P-value<0.0001)**

In vivo results: According to the macroscopic images presented in Figure 7I and 7II, the visual examination of the images shows the therapeutic effect of the optimal group, i.e. the combination of carbomer 980 and HPMC with GO NPs, ZnO and ZnS, compared to the control group. In addition, no significant effect of infection was observed in any of the groups. Next, in order to evaluate the wound healing and the progress of the healing stages, the rate of wound closure was examined (Figure 7III). The results showed that the optimal group was significantly cured compared to the control group.

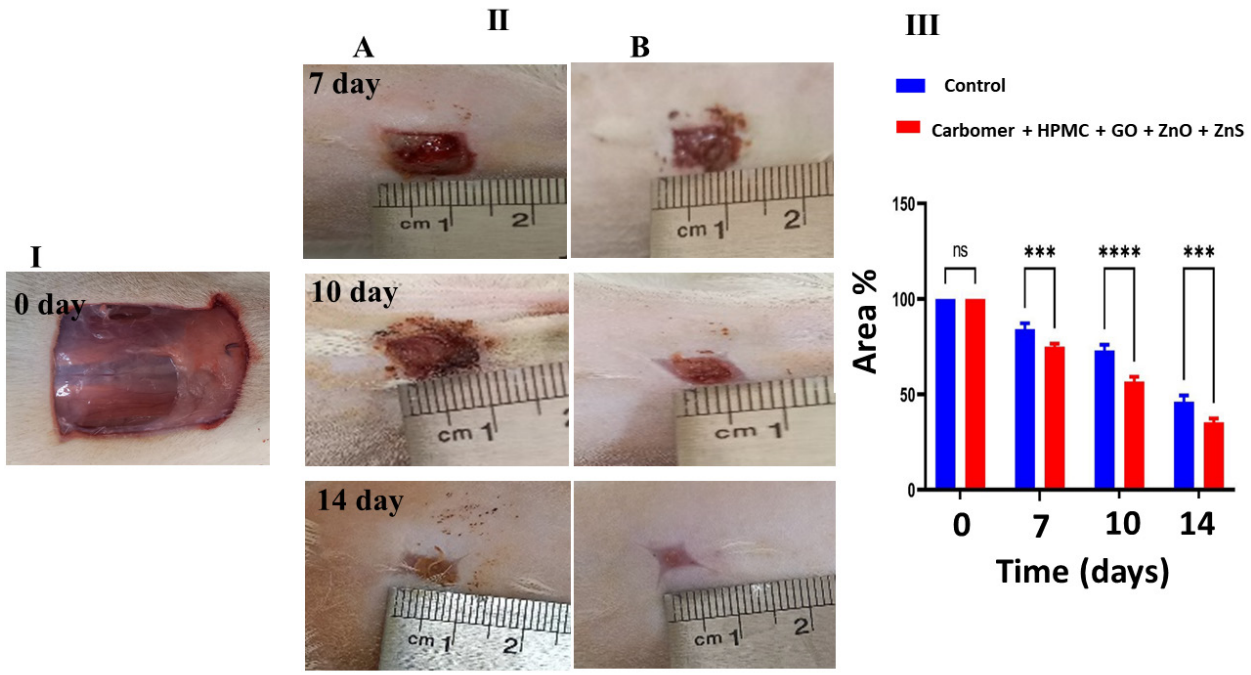

Figure 7. Evaluation of wound closure. Macroscopic images of I control group and II healing wound after 7, 10 and 14 days. III: Diagram of wound closure

(**P-value<0.0001)**

Hematoxylin-eosin and Verhof van Gieson staining results: In this study, after treating mice with carbomer 980 and HPMC containing GO NPs, ZnO and ZnS for 14 days, tissue samples were preserved in 10% formalin after cutting and then the tissue slides were stained. Investigations showed that skin regeneration was completed within 24 days. H&E staining results (Figure 8I) show that in the group treated with carbomer 980 and HPMC containing GO NPs, ZnO and ZnS, wound regeneration was similar to the positive control group and epidermal regeneration and blood vessel formation were higher in this group than in other groups. In addition, the formation of hair follicles, sebaceous glands and normal epidermis was higher in this group than in other groups. Also, according to the results, the rate of collagen fiber synthesis and collagen deposition in this group reached a maximum. Based on the results obtained from Verhof van Gieson staining (Figure 8II), the group treated with carbomer 980 and HPMC containing GO NPs, ZnO, and ZnS had more elastin fiber formation and mature collagen formation than the other groups.

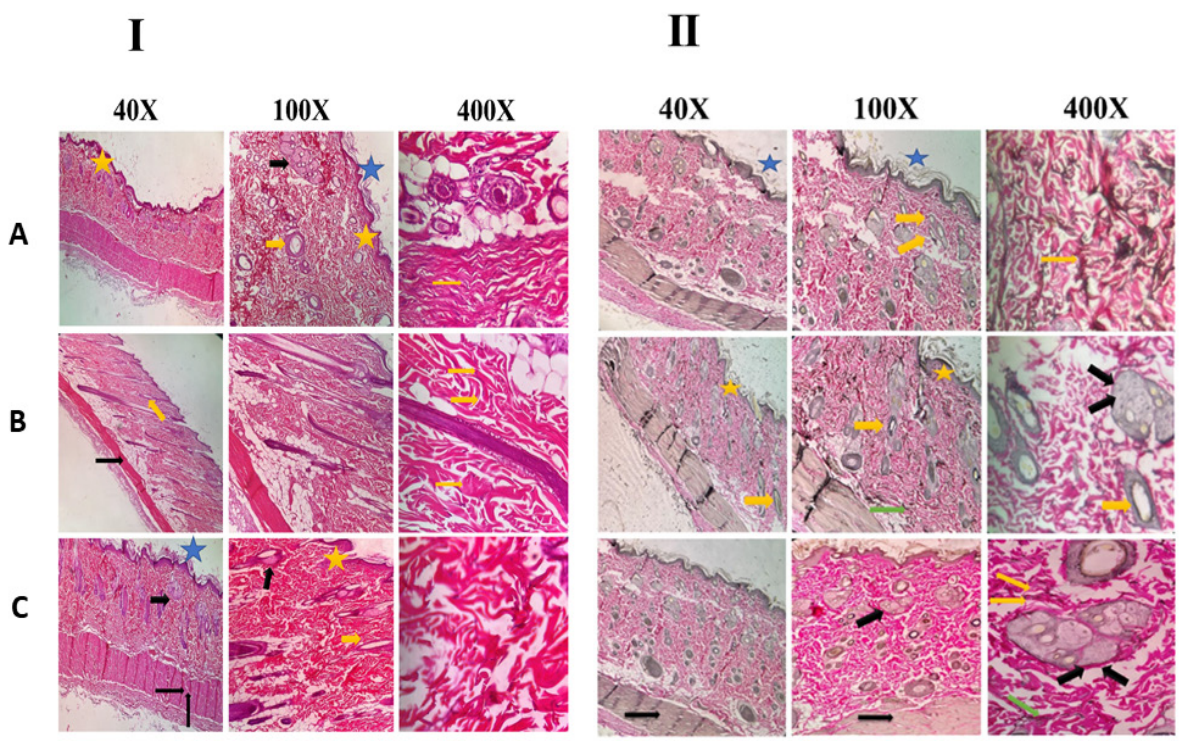

Figure 8. I: Results of hematoxylin-eosin and Verhof van Gieson staining in this study. A: Negative control group. B: Positive control group. C: Group treated with carbomer 980 and HPMC containing GO, ZnO and ZnS NPs (magnification 40X, 100X, 400X).

(Blue star indicates dead skin, yellow star indicates epithelium, wide yellow arrow indicates hair follicle, wide black arrow indicates sebaceous glands, narrow black arrow indicates angiogenesis and yellow arrow indicates mature collagen and narrow green arrow indicates elastin fibers.)

Discussion

Hydrogels with high water content are largely biocompatible and have mechanical properties similar to soft tissues, which allow cells and bioactive molecules to be easily incorporated during the gelation process [19]. Due to these properties, these polymers have been widely used in wound healing [20]. Carbomer 980 is a biocompatible hydrogel that enhances cell viability through its carboxylic groups (-COOH), which promote cell adhesion via hydrogen bonding and electrostatic interactions, while also helping maintain a near-physiological pH (~7.4). Its high water absorption capacity provides a hydrated environment that reduces cellular stress. Compared to HPMC, which lacks active functional groups, carbomer 980 offers stronger adhesion, higher biocompatibility, and more direct support for cell growth and repair. Consequently, cytotoxicity tests typically show greater cell viability with carbomer than with HPMC [21]. Our findings demonstrate that carbomer–HPMC composites containing GO exhibit superior biocompatibility compared to those with ZnO or ZnS NPs. This advantage arises from the unique physicochemical properties of GO and its interactions with the polymer matrix. GO's two-dimensional structure and high surface area enable strong polymer binding and cell interactions, thereby promoting adhesion and proliferation without inducing cytotoxic effects. In contrast, ZnO and ZnS reduce cell viability primarily through oxidative stress. ZnO, with its pronounced photocatalytic activity, generates ROS under UV exposure, leading to DNA, protein, and lipid damage. ZnS, though less photocatalytically active, still contributes to oxidative stress via Zn^{2+} ion release. These mechanisms explain the lower survival rates observed in MTT, DAPI, and scratch assays for ZnO- and ZnS-based formulations compared to GO-based composites [22, 23].

FTIR analysis confirmed that the main chemical structures of the polymers and NPs were preserved, while minor peak shifts suggested interactions between components—consistent with previous reports [24-33]. Hematological evaluations further supported the biocompatibility of graphene-based formulations. Swelling tests showed that all nanoparticle-containing Carbomer (980) and HPMC formulations absorbed large amounts of water, attributed to the polymers' hydrophilic groups, the high surface area of NPs, and the formation of 3D polymer–nanoparticle networks that facilitate moisture retention. Weight loss studies revealed faster degradation in nanoparticle-loaded samples, likely due to their larger surface area, increased water uptake, and functional group activation, which accelerate polymer breakdown. Carbomer (980), a high-molecular-weight acrylic polymer with 56–68% carboxyl groups (–COOH), swells extensively in aqueous environments due to ionization of its side chains. In combination with GO NPs, Carbomer and HPMC demonstrated strong wound-healing potential in animal models. This effect can be

explained by: 1. High biocompatibility of GO, which supports tissue repair, cell migration, and collagen formation. 2. Polymeric structural support, where Carbomer and HPMC provide a scaffold for fibroblast and epidermal cell migration, enhancing repair. 3. Synergistic physical–chemical properties, with GO's nanostructure and large surface area improving polymer interactions and healing outcomes. 4. Antioxidant activity of GO, which reduces oxidative stress. 5. Moisture retention, as the polymer–nanoparticle system maintains a moist wound environment that accelerates healing.

Overall, the combined use of GO, ZnS, and ZnO NPs with Carbomer 980 and HPMC produced better outcomes than NPs alone, highlighting the synergistic role of polymers and NPs in both in vitro and in vivo wound-healing models.

This study has some limitations that should be acknowledged. The experiments were conducted on a relatively small sample size with a short follow-up period, which may restrict the generalizability of the findings. In addition, the absence of clinical translation limits the direct application of the results to human patients. Future studies with larger cohorts, longer observation times, and clinical investigations will be essential to validate the therapeutic potential of GO-based hydrogels.

Conclusion: The results of this study showed that the combination of GO NPs with carbomer (980) and HPMC effectively improved antioxidant effects and reduced cell damage. These compounds were successful in reducing oxidative stress and the level of released LDH and prevented damage caused by ROS. GO NPs, along with carbomer (GO) and HPMC polymers, are able to reduce oxidative stress and protect cell membranes in vitro and in animal models due to their unique properties such as large surface area, high stability and biocompatibility. In addition, these compounds showed improvement in wound healing and cell migration in animal models, which was due to the chemical and physical properties of NPs and polymers. Therefore, the combination of GO NPs with these polymers is suggested as an effective system for therapeutic applications such as wound healing and improving antioxidant and biological properties of tissues. These results could lead to the development of new materials in medical and biological therapies.

Future approaches: Future research should focus on designing advanced combinations of NPs with polymers such as carbomer or HPMC to enhance wound healing and antioxidant activity. A deeper investigation of the molecular and cellular pathways involved in tissue repair and inflammation is also needed to clarify the therapeutic effects. In addition, GO and other NPs combined with polymers could be utilized as carriers for anti-inflammatory agents, antibiotics, or growth stimulants in drug delivery systems. Comprehensive studies on toxicity, immune response, and overall safety of nanoparticle–polymer systems are essential to ensure their suitability for clinical applications. Furthermore, developing innovative hydrogels, nanocomposites, and nanostructured films can significantly improve the efficiency and applicability of wound healing therapies.

Ethical Considerations

All animal experiments and biological assessments in this study were conducted in strict accordance with the guidelines of the ARRIVE (Animal Research: Reporting of In Vivo Experiments), the U.K. Animals (Scientific Procedures) Act, 1986, EU Directive 2010/63/EU for animal experiments, and the National Institutes of Health Guide for the Care and Use of Laboratory Animals (NIH Publications No. 8023, revised 1978). The experimental protocol was approved by the Shahroud University of Medical Sciences (Approval Number: IR.SHMU.REC.1401.166).

Acknowledgment

The authors would like to thank Shahroud University of Medical Sciences for providing laboratory facilities.

Conflict of Interest

All authors have given approval for the final version of the manuscript. The authors declare that they have no conflict of interest.

Funding

This study was supported by grant No 14010049 and ethics number IR.SHMU.REC.1401.166 from Shahroud University of Medical Sciences.

References

1. Reinke J, Sorg HJEsr. Wound repair and regeneration. 2012;49(1):35-43. doi: 10.1159/000339613

2. Motley TA, Gilligan AM, Lange DL, Waycaster CR, Dickerson JEJJoF, Research A. Cost-effectiveness of clostridial collagenase ointment on wound closure in patients with diabetic foot ulcers: economic analysis of results from a multicenter, randomized, open-label trial. 2015;8:1-12. doi: 10.1186/s13047-015-0065-x

3. Boyce ST, Lalley ALJB, trauma. Tissue engineering of skin and regenerative medicine for wound care. 2018;6 doi: 10.1186/s41038-017-0103-y

4. Alavi A, Sibbald RG, Mayer D, et al. Diabetic foot ulcers: part II. Management. 2014;70(1):21. e1-21. e24. doi: 10.1016/j.jaad.2013.07.048

5. Fajriyah NN, Slamet S, Waznah U, et al. Topical nano hydrogel formulation of annona muricata extract enrich with zinc for improved therapy design and evaluation. AIP Publishing; 2023: doi: 10.1063/5.0120738

6. Jaworski Z, Spychaj T, Story A, Story GJRiCE. Carbomer microgels as model yield-stress fluids. 2022;38(7):881-919. doi: 10.1515/revce-2020-0016

7. Dahl T, Calderwood T, Bormeth A, Trimble K, Piepmeier EJJocr. Influence of physico-chemical properties of hydroxypropyl methylcellulose on naproxen release from sustained release matrix tablets. 1990;14(1):1-10. doi: 10.1016/0168-3659(90)90055-X

8. Siepmann J, Peppas NAJAddr. Modeling of drug release from delivery systems based on hydroxypropyl methylcellulose (HPMC). 2012;64:163-174. doi: 10.1016/j.addr.2012.09.028

9. Hajipour MJ, Fromm KM, Ashkarran AA, et al. Antibacterial properties of nanoparticles. 2012;30(10):499-511. doi: 10.1016/j.tibtech.2012.06.004

10. Kalpana V, Devi Rajeswari VJBc, applications. A review on green synthesis, biomedical applications, and toxicity studies of ZnO NPs. 2018;2018(1):3569758. doi: 10.1155/2018/3569758

11. Han B, Fang WH, Zhao S, Yang Z, Hoang BXJNN, Biology, Medicine. Zinc sulfide nanoparticles improve skin regeneration. 2020;29:102263. doi: 10.1016/j.nano.2020.102263

12. Kaushik M, Niranjan R, Thangam R, et al. Investigations on the antimicrobial activity and wound healing potential of ZnO nanoparticles. 2019;479:1169-1177. doi: 10.1016/j.apsusc.2019.02.189

13. Shirshahi V, Tabatabaei SN, Hatamie S, Saber RJJoP, Analysis B. Functionalized reduced graphene oxide as a lateral flow immuneassay label for one-step detection of Escherichia coli O157: H7. 2019;164:104-111. doi: 10.1016/j.jpba.2018.09.048

14. Saedi M, Shirshahi V, Mirzaii M, Nikbakht MJJoDS, Technology. Preparation of graphene oxide nanoparticles and their derivatives: Evaluation of their antimicrobial and anti-proliferative activity against 3T3 cell line. 2024;45(3):381-389. doi: 10.1080/01932691.2022.2151458

15. Shirshahi V, Saedi M, Nikbakht M, Mirzaii MJJoDDS, Technology. Unveiling the antimicrobial potential of oxidized graphene derivatives: promising materials for advanced wound dressings and antibacterial surfaces. 2023;88:104949. doi: 10.1016/j.jddst.2023.104949

16. Ma R, Wang Y, Qi H, et al. Nanocomposite sponges of sodium alginate/graphene oxide/polyvinyl alcohol as potential wound dressing: In vitro and in vivo evaluation. 2019;167:396-405. doi: 10.1016/j.compositesb.2019.03.006

17. Mahmoudi N, Eslahi N, Mehdipour A, et al. Temporary skin grafts based on hybrid graphene oxide-natural biopolymer nanofibers as effective wound healing substitutes: pre-clinical and pathological studies in animal models. 2017;28:1-13. doi: 10.1007/s10856-017-5874-y

18. Karimi F, Alizadeh M, Bitaraf FS, Shirshahi V. Enhancing electrical conductivity and mechanical properties of decellularized umbilical cord arteries using graphene coatings. Journal of Biomedical Materials Research Part B: Applied Biomaterials 2024;112(7):e35448. doi: 10.1002/jbm.b.35448

19. Agubata CO, Okereke C, Nzekwe IT, Onoja RI, Obitte NCJEJoPS. Development and evaluation of wound healing hydrogels based on a quinolone, hydroxypropyl methylcellulose and biodegradable microfibres. 2016;89:1-10. doi: 10.1016/j.ejps.2016.04.017

20. Prabu D, Majdalawieh AF, Abu-Yousef IA, et al. Preparation and characterization of gatifloxacin-loaded sodium alginate hydrogel membranes supplemented with hydroxypropyl methylcellulose and hydroxypropyl cellulose polymers for wound dressing. 2016;6(2):86. doi: 10.4103/2230-973X.177810

21. Ismail SH, Hamdy A, Ismail TA, Mahboub HH, Mahmoud WH, Daoush WMJC. Synthesis and characterization of antibacterial carbopol/ZnO hybrid nanoparticles gel. 2021;11(9):1092. doi: 10.3390/cryst11091092

22. Kaushik M, Niranjan R, Thangam R, et al. Investigations on the antimicrobial activity and wound healing potential of ZnO nanoparticles. Applied Surface Science 2019;479:1169-1177. doi: 10.1016/j.apsusc.2019.02.189

23. Cleetus CM, Alvarez Primo F, Fregoso G, et al. Alginate hydrogels with embedded ZnO nanoparticles for wound healing therapy. International journal of nanomedicine 2020:5097-5111. doi: 10.2147/IJN.S255937

24. Wang Z, Hu Y, Xue Y, et al. Log P determines licorice flavonoids release behaviors and classification from CARBOMER cross-linked hydrogel. 2022;14(7):1333. doi: 10.3390/pharmaceutics14071333

25. Wang Z, Xue Y, Zhu Z, et al. Quantitative structure-activity relationship of enhancers of licochalcone a and glabridin release and permeation enhancement from carbomer hydrogel. 2022;14(2):262. doi: 10.3390/pharmaceutics14020262

26. Zaltariov M-FJCCTCCT. FTIR investigation on crystallinity of hydroxypropyl methyl cellulose-based polymeric blends. 2021;55:981-988. doi: 10.35812/CelluloseChemTechnol.2021.55.84

27. Surekha G, Krishnaiah KV, Ravi N, Suvarna RP. FTIR, Raman and XRD analysis of graphene oxide films prepared by modified Hummers method. IOP Publishing; 2020:012012. doi: 10.1088/1742-6596/1495/1/012012

28. El-Belely EF, Farag MM, Said HA, et al. Green synthesis of zinc oxide nanoparticles (ZnO-NPs) using Arthrospira platensis (Class: Cyanophyceae) and evaluation of their biomedical activities. 2021;11(1):95. doi: 10.3390/nano11010095

29. Abdelghany A, Meikhail M, Oraby A, Aboelwafa MJPB. Experimental and DFT studies on the structural and optical properties of chitosan/polyvinyl pyrrolidone/ZnS nanocomposites. 2023;80(12):13279-13298. doi: 10.1007/s00289-023-04700-0

30. Gharagozlou M, Naghibi SJMRB. Sensitization of ZnO nanoparticle by vitamin B12: Investigation of microstructure, FTIR and optical properties. 2016;84:71-78. doi: 10.1016/j.materresbull.2016.07.029

31. Pouran HM, Llabjani V, Martin FL, Zhang HJEs, technology. Evaluation of ATR-FTIR spectroscopy with multivariate analysis to study the binding mechanisms of ZnO nanoparticles or Zn2+ to chelex-100 or metsorb. 2013;47(19):11115-11121. doi: 10.1021/es4017552

32. Praseptiangga D, Zahara HL, Widjanarko PI, Joni I, Panatarani C. Preparation and FTIR spectroscopic studies of SiO2-ZnO nanoparticles suspension for the development of carrageenan-based bio-nanocomposite film. AIP Publishing; 2020: doi: 10.1063/5.0003434

33. Srujana S, Bhagat DJNfEE. Chemical-based synthesis of ZnO nanoparticles and their applications in agriculture. 2022;7(1):269-275. doi: 10.1007/s41204-022-00224-6